Journal of Biomedical Optics

BiomedicalOptics.SPIEDigitalLibrary.org

# Intravital live cell triggered imaging system reveals monocyte patrolling and macrophage migration in atherosclerotic arteries

Sara McArdle
Grzegorz Chodaczek
Nilanjan Ray
Klaus Ley

SPIE.

# Intravital live cell triggered imaging system reveals monocyte patrolling and macrophage migration in atherosclerotic arteries

**Sara McArdle,[a,b] Grzegorz Chodaczek,[a,c] Nilanjan Ray,[d] and Klaus Ley[a,*]**
[a]La Jolla Institute, 9420 Athena Circle, La Jolla, California 92037, United States
[b]University of California, Department of Bioengineering, San Diego, 9500 Gilman Drive, La Jolla, California 92093, United States
[c]Wroclaw Research Centre EIT+, Stabłowicka 147, 54-066 Wroclaw, Poland
[d]University of Alberta, Department of Computing Science, 8900 114 Street Northwest, Edmonton, Alberta T6G 2S4, Canada

**Abstract.** Intravital multiphoton imaging of arteries is technically challenging because the artery expands with every heartbeat, causing severe motion artifacts. To study leukocyte activity in atherosclerosis, we developed the intravital live cell triggered imaging system (ILTIS). This system implements cardiac triggered acquisition as well as frame selection and image registration algorithms to produce stable movies of myeloid cell movement in atherosclerotic arteries in live mice. To minimize tissue damage, no mechanical stabilization is used and the artery is allowed to expand freely. ILTIS performs multicolor high frame-rate two-dimensional imaging and full-thickness three-dimensional imaging of beating arteries in live mice. The external carotid artery and its branches (superior thyroid and ascending pharyngeal arteries) were developed as a surgically accessible and reliable model of atherosclerosis. We use ILTIS to demonstrate *Cx3cr1*$^{GFP}$ monocytes patrolling the lumen of atherosclerotic arteries. Additionally, we developed a new reporter mouse (*Apoe*$^{-/-}$*Cx3cr1*$^{GFP/+}$*Cd11c*$^{YFP}$) to image GFP+ and GFP+YFP + macrophages "dancing on the spot" and YFP+ macrophages migrating within intimal plaque. ILTIS will be helpful to answer pertinent open questions in the field, including monocyte recruitment and transmigration, macrophage and dendritic cell activity, and motion of other immune cells.  [DOI: 10.1117/1.JBO.20.2.026005]

Keywords: intravital microscopy; multiphoton microscopy; triggering; registration; atherosclerosis; monocytes.

Paper 140757R received Nov. 14, 2014; accepted for publication Jan. 12, 2015; published online Feb. 24, 2015.

## 1 Introduction

Intravital optical imaging is an invaluable tool for accurately studying biological and disease processes. However, imaging live animals introduces technical challenges due to motion artifacts, especially in cardiovascular organs that are inherently subject to vigorous motion. One such tissue with significant medical relevance and that is still largely unexplored is atherosclerotic arteries. In the course of atherosclerosis artery walls become infiltrated over time by various immune cells such as macrophages, dendritic cells, T lymphocytes, and other inflammatory cells.[1] Dynamic intravital visualization of these processes at the cellular and subcellular levels still awaits its realization due to difficulties with access to the vessel luminal side and image stability during the acquisition. Two-photon microscopy is the only type of fluorescent microscopy that can image through the depth of the atherosclerotic plaque, which can be 100- to 200-$\mu$m thick. Additionally, in a living mouse, large arteries expand and contract with every heartbeat, moving the wall vertically and laterally, which severely compromises the image quality. Motivated by the need to visualize recruitment of inflammatory cells from the blood and monitor the movement of macrophages inside the plaque we developed and refined a new intravital live cell triggered imaging system (ILTIS), which has the potential to study the process of atherosclerosis *in vivo* with high quality and subcellular resolution. Because commonly studied areas of plaque development, including the aortic arch and carotid artery bifurcation, were not suitable for these purposes, we developed a new model based on a more accessible artery, a branch of the external carotid (EC) artery.

There are three commonly used methods for minimizing motion artifacts in intravital laser scanning microscopy of tissues with innate motion, such as the heart or lungs: mechanical stabilization, triggering, and image postprocessing.[2] Various techniques have been successfully used to physically restrain tissue movement, such as tissue glue,[3–5] compression,[6,7] or suction[8–10] to attach a stabilizer. However, these methods are not suitable for arterial preparations. The cylindrical geometry of the artery makes a suction ring approach infeasible. Also, the artery wall, especially the adventitia, is a delicate tissue that may be damaged by tissue glue. In contrast, triggered acquisition enables high-resolution imaging while allowing the tissue to move freely by only acquiring data when the tissue is in a quasisteady position. Alternatively, triggering can also be done in a retrospective manner, where data are acquired continuously while the heartbeat and breathing are recorded and then only images or image fractions that were acquired within predetermined windows in both cycles are kept. Triggering based on heartbeat and respiration has been used to image healthy arteries; however, to date the use of this technique alone has been limited to image a single plane in animals with low heart rates, such as rats or deeply anesthetized mice.[11] Triggering has also been used to improve two-dimensional

*Address all correspondence to: Klaus Ley, E-mail: klaus@liai.org

1083-3668/2015/$25.00 © 2015 SPIE

(2-D)[4,10] and three-dimensional (3-D) imaging of the heart[3,6] and carotid artery[7] that was predominantly stabilized mechanically. The third method, postprocessing, is applied after data collection to remove motion artifacts by selecting for further analysis only a fraction of the acquired images based on apparent motion in the images themselves.[12] Just as with retrospective triggering, relying on postprocessing alone can lead to phototoxicity and photobleaching because the tissue is exposed to extra excitation light that will never be used for analysis; however, it has been successfully combined with mechanical stabilization to produce high-quality movies of various organs.[13]

Multiphoton imaging of leukocytes in mouse arteries was pioneered by the Weber/Sohnlein group.[12] The authors used an instrument (LaVision TrimScope) that was state-of-the-art at the time and detected $Lysm^{GFP}$-labeled neutrophils adherent to the lumen of the common carotid artery. Some neutrophils appeared to be crawling into what may be plaque tissue. However, no other cells or structures were labeled except collagen by second-harmonic generation (SHG) and elastin by autofluorescence, so the location of these neutrophils remains unclear. Statistical analysis was not possible because only a single experiment was reported in their study. Frames were manually selected without proper registration, making it difficult to distinguish cell motion apart from motion artifacts due to focal plane changes.

The same group together with Hidalgo and Andres published a refined method of imaging neutrophils in atherosclerosis.[7] Mechanical stabilization achieved by restraining the carotid artery between a metal holder and a coverslip limited the vessel wall excursions due to the heartbeat. Respiratory motion was removed by triggered acquisition. The authors reported one experiment with $Lysm^{GFP}$ mice in which a Leica SP5 II microscope was used to image neutrophils, collagen, and the plasma volume. In a shallow stack (total thickness 18 $\mu$m), the authors showed what appeared to be neutrophil crawling on the endothelial surface, similar to what was previously reported in microvessels.[14] However, it is unclear what effect the mechanical stabilization had on the cell behavior.

To image live cells in a large volume of the freely beating atherosclerotic artery, we developed ILTIS, a novel technique that relies predominantly on cardiac triggering followed by image selection and registration to remove residual artifacts, without any mechanical stabilization. This system was used to image cells in the EC, superior thyroid (ST), and ascending pharyngeal (AP) arteries of $Apoe^{-/-}$ mice fed a high-fat "Western diet" (WD), a commonly used model of atherosclerosis.[15] This method can be applied in two modes: high time resolution 2-D, or full wall thickness 3-D imaging. Taking advantage of $Cx3cr1^{GFP}$ mice,[16] in which all nonclassical monocytes are labeled with GFP, we were repeatedly able to demonstrate monocytes crawling on the endothelium in the lumen of atherosclerotic arteries. To image macrophages in the vessel associated with the plaque, we generated double transgenic mice that express YFP under the CD11c promoter[17] and GFP under the Cx3cr1 promoter. Macrophages accumulated in atherosclerotic lesion showed two types of behaviors: some YFP+ cells moved substantial distances (up to 100 $\mu$m), whereas most GFP+ and GFP+YFP+ cells within the artery wall extended and retracted dendritic processes and showed a "dancing on the spot" behavior. This and other phenomena revealed through ILTIS will definitely help in further investigations and in our understanding of atherosclerosis.

## 2 Materials and Methods

### 2.1 *Mice*

$Apoe^{-/-}$ mice were obtained from Jackson Laboratories. $Cd11c^{YFP}$ mice were provided by M. Nussenzweig (Rockefeller University, New York).[17] $Cx3cr1^{GFP}$ mice were provided by S. Jung (Weizmann Institute of Science, Israel).[16] Mice were kept in specific pathogen-free conditions in an AAALAC-approved barrier facility, and all experiments were performed in accordance with IACUC standards. $Cd11c^{YFP}$ mice and $Cx3cr1^{GFP}$ mice were both bred onto the $Apoe^{-/-}$ background. The independent strains were then bred to each other to create the $Cx3cr1^{GFP/+}$ $Cd11c^{YFP}$ $Apoe^{-/-}$ strain used in this study. For these experiments, only the $Cx3cr1^{GFP/+}$ genotype was used to exclude any potential effects associated with deletion of *Cx3cr1* gene in homozygous mice.[18] All three combinations of genotypes were used in the study: $Cx3cr1^{GFP/+}$ $Cd11c^{YFP}$, $Cx3cr1^{GFP/+}$, and $Cx3cr1^{WT/WT}$ $Cd11c^{YFP}$. The $Cd11c^{YFP}$ transgene was screened using the following primers for *CD11c* and *YFP*, respectively: 5′-TGC TGG TTG TTG TGC TGT CTC ATC-3′ and 5′-GGG GGT GTT CTG CTG GTA GTG GTC-3′.The *Cx3cr1* wild type allele was screened for using the following primers: 5′-TTC ACG TTC GGT CTG GTG GG-3′ and 5′-CGT CTG GAT GAT TCG GAA GTA GC-3′. The GFP knock-in construct was screened with the following primers: 5′-TAA ACG GCC ACA AGT TCA GCG-3′ and 5′-TAC TCC AGC TTG TGC CCC AGG ATG TT-3′. RT-PCR testing was conducted by Transnetyx. All mice were fed WD starting at 6 to 8 weeks of age.

### 2.2 *Histology and Immunofluorescence*

The right EC artery from an $Apoe^{-/-}$ mouse fed WD for 9 weeks was dissected from the branch point toward the internal carotid artery to the edge of the visible plaque of the ST, AP, and EC arteries and embedded in optimal cutting temperature compound. Serial 5-$\mu$m cross sections were cut on a cryostat. Sections, every 30 $\mu$m throughout the length of the visible plaque, were stained with Oil Red O, Trichrome and H&E using standard procedures. Sections were stained for CD11b (biotinylated rat anti-mouse, BD Pharmingen, M1/70, 1:100) and CD11c (hamster anti-mouse, BD Pharmingen, HL3, 1:20), or $\alpha$-smooth muscle actin ($\alpha$SMA) (polyclonal rabbit anti-mouse, Abcam, 1:1000) overnight. The secondary antibodies were: streptavidin-Alexa Fluor 555 (Invitrogen, 1:500), anti-hamster-Alexa Fluor 633 (Jackson IR, 1:250), and anti-rabbit-Alexa Fluor 594 (Invitrogen, 1:500). Directly conjugated APC-rat anti-mouse CD31 (BD Pharmingen, Mec13.3, 1:100) was added to the slides stained for $\alpha$SMA. Nuclei were stained with Yoyo-1 (Invitrogen).

### 2.3 *Surgery*

Mice were anesthetized with a standard mixture of ketamine/xylazine/atropine (100/10/0.4 mg/kg intraperitoneally). Fur on the thigh and anterior neck was removed with depilatory cream and then the skin was washed with 70% ethanol to remove the cream. Saline was injected intraperitoneally (0.5 mL) to protect the mouse from dehydration. A 2 cm craniocaudal opening was cut in the anterior neck. The salivary glands were separated, and then moved to each side and weighed down with tissue clamps. The muscle surrounding the trachea was cut away, and a tracheal cannula (PE90) was

placed and tied securely. The left jugular vein was cleaned of fat, and a cannula (PE10 with a 28G needle) was inserted and tied. For extra security, the jugular vein cannula was secured with tissue glue. Supplemental anesthetic was applied at 20- to 30-min intervals via the jugular vein catheter as needed. The ligament of the right sternomastoideus muscle was cut and the proximal end of the muscle was pulled away from the right carotid artery and secured with a tissue clamp. Extraneous tissue around the EC artery was removed without touching the thin fascia covering the artery.

### 2.4 *Multiphoton Microscopy*

All imaging experiments were conducted on a Leica SP5 with a water-dipping objective (Olympus XLUMPLFL 20X NA 0.95). The system is composed of a DM6000 microscope, a Ti-Sapphire laser (Chameleon Ultra II, Coherent), tuned to 920 nm for all experiments, a resonant scanhead for fast scanning, and a Leica trigger box. The emitted light was split into three photomultiplier tube detectors by two dichroic mirrors (520 and 495 nm) and three filters (513/17 nm for GFP, 513/22 nm for YFP, and 460/50 for collagen visualized by SHG).

Acquired images cover 512 pixels in $x$ (the vessel axis) and 200 to 256 pixels in $y$, depending on heart rate. All images used 3-6$x$ line scan averaging, for a total of 35 to 70 ms/frame. The $xy$ pixels were isotropic at 890 nm/pixel. We chose to acquire a large field of view at the expense of maximum spatial resolution.

During the imaging, the imaged area was kept wet by with a slow drip (5 to 10 mL/h) of superfusion fluid [Roswell Park Memorial Institute medium (RPMI) without phenol red] from a syringe pump [Fig. 1(a)]. The mouse was warmed to 37°C with a heating pad on a feedback loop while an objective heater (OW-2D, Warner) heats both the objective and the superfusion fluid [Fig. 1(a)]. Preliminary experiments showed that injectable anesthesia resulted in a reduction of the heart rate to ~350 bpm, but also caused low tissue oxygen saturation and arrhythmias as measured by the pulse oximeter. Reducing the heart rate with anesthesia is desirable because it lengthens the diastolic phase, allowing for more time to acquire a frame. Oxygen saturation improved to 98% and arrhythmias were reduced when the mice were given supplemental oxygen next to the cannulated trachea.

### 2.5 *Triggered Imaging*

In order to achieve triggered acquisition, the mouse heartbeat needs to "drive" the microscope. Figure 1 describes the setup and workflow for achieving triggered acquisition. The trigger pulse is derived from a pulse oximeter (MouseOx, Starr Life Sciences) placed on the thigh of the mouse [Fig. 1(a)], using the output that reflects oxygenated hemoglobin [Fig. 1(b)]. The analog pulse wave signal is conditioned in a simple custom-built heartbeat detection circuit, utilizing an Arduino microcontroller (Duemilanove, Smartprojects) [Fig. 1(a)]. Systole is detected when the pulse oximeter output goes from positive to negative [Fig. 1(b)]. Since the heartbeat signal is acquired at a different location from the imaged area, an adjustable delay circuit is implemented to ensure that image acquisition proceeds during effective diastole [Figs. 1(b) and 1(c)]. The delay (typically 0 to 30 ms) is adjusted manually until the apparent motion between frames is minimal. After the delay, the microcontroller produces a trigger pulse that is fed into

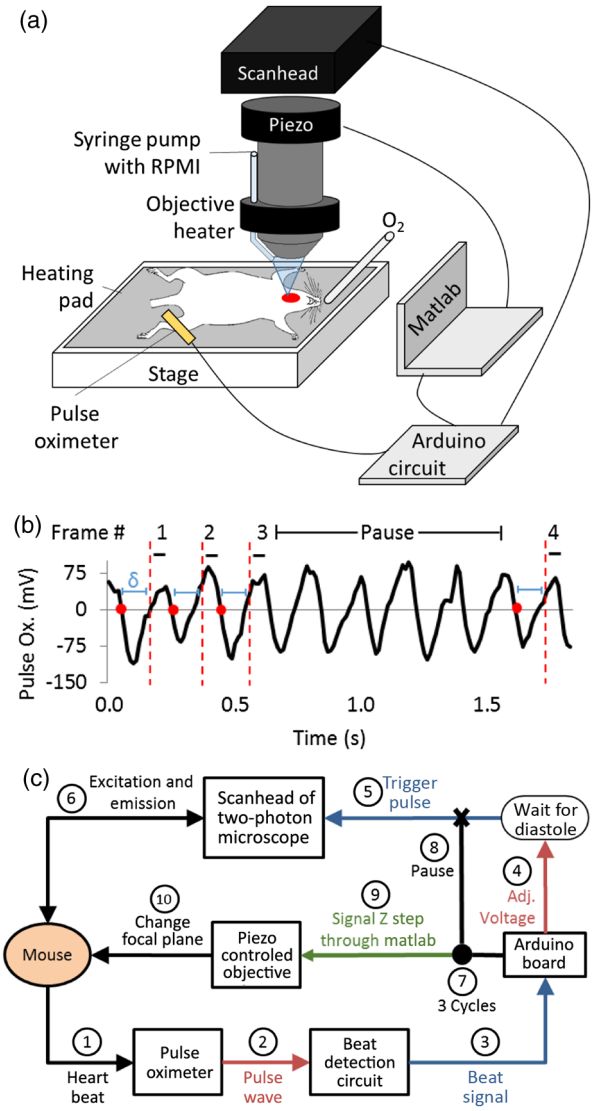


**Fig. 1** (a) Schematic diagram of intravital live cell triggered imaging system (ILTIS) setup. The mouse is placed supine on a heating pad on the microscope stage, and is breathing freely with additional oxygen provided. A syringe pump pumps RPMI into the space between the carotid artery and the objective and both the liquid and the objective are kept warm with an objective heater. The mouse's heartbeat is monitored by a pulse oximeter on the mouse's thigh, which is connected through the Arduino microcontroller circuit to the scanhead of the two-photon microscope. The position of the objective is controlled by a piezo-actuator, which is in communication with MATLAB and the heartbeat detection circuit. (b) Illustration of triggered image acquisition in response to the heartbeat, showing representative output from the pulse oximeter (black line), detection of a heartbeat when pulse oximeter signal become negative (dot), adjustable delay time after heartbeat detection (labeled $\delta$, thin line), representation of trigger pulse sent to Leica trigger box (dotted line), and ~50 ms image acquisition time during diastole (black bars above pulse oximeter graph). (c) Control diagram of triggering system. Arrows show direction of information flow. The mouse's heartbeat is monitored by the pulse oximeter (1), which outputs an analog signal (2). The waveform is digitized (3) and sent to an Arduino microcontroller, which after an adjustable delay (4) outputs a trigger pulse (5) to the microscope to acquire an image (6). This repeats three times (7), and then the Arduino suppresses all trigger signals for 1 s (8) to reduce photobleaching. For three-dimensional (3-D) imaging, the Arduino also signals through MATLAB to the piezo-actuator (9) to change the focal plane (10). Red lines (2,4)—analog signals, blue lines (3,5)—digital signals, and green lines (9)—serial communication.

the microscope scanhead using a Leica trigger box and initiates acquisition of a single frame [Fig. 1(b)]. The process is then repeated at the next heartbeat.

Three (occasionally four) images in consecutive heartbeats were acquired, and then a short pause was inserted to reduce photobleaching [Figs. 1(b) and 1(c)]. In postprocessing, one out of each triplet of frames was automatically chosen to compile the final movie (see below).[19] For 2-D movies, a 1 s pause was inserted. This time was chosen to be fast enough (average final rate of 0.66 Hz) to accurately track cells between frames but still allow for 30 to 45 min movies with minimal photobleaching. For 3-D movies, in between each triplet of frames, the Arduino microcontroller sent a signal through MATLAB to the nosepiece piezo-controller (Piezosystem Jena, NV 40/1 CLE and MIPOS 500 SG) on the microscope objective to change the imaging focal plane [Figs. 1(a) and 1(c)]. The inserted pause in this case was only 300 ms (approximately 1 heartbeat). Stacks of 25 to 40 Z slices were acquired, with a final frame rate of approximately one stack every 42 s. After one out of each triplet of frames was selected, image registration was used to reduce residual motion. These postprocessing algorithms effectively remove artifacts due to respiration along with those from other unknown sources.

### 2.6 *Image Selection Method in 3-D Experiments*

The image selection problem is defined as follows. If there are $M$ 2-D images in each Z-stack (spatial direction) and $N$ Z-stacks (time direction) in total, with $K$ images acquired at every space-time location, the exhaustive search space to select one image per location is enormous: $K^{MN}$. To reduce this computational complexity, it is natural to impose similarity among images acquired at neighboring locations in the space-time grid, much like Markov random field type modeling in image analysis.[20] Thus, while selecting an image at $i$'th spatial location and $j$'th time point, we would like to impose its similarity with images acquired at $(i+1,j)$'th, $(i-1,j)$'th, $(i,j+1)$'th, and $(i,j-1)$'th locations. To formulate this pairwise similarity within a sound mathematical framework, consider $I_{i,j,n}$ to be the $n$'th of the $K$ images acquired at location $(i,j)$. The image selection problem is then to select one out of $K$ images at every $(i,j)$ location in the space-time grid. The aforementioned image selection problem with pairwise similarity on the 2-D space-time grid can now be formulated as a minimization of the following cost function with respect to binary variables $a_{i,j,n}$:

$$\min \sum_{(i,j),(k,l):|i-k|+|j-l|=1} \sum_{n=1}^{K} \sum_{m=1}^{K} a_{i,j,n} a_{k,l,m} \|I_{i,j,n} - I_{k,l,m}\|,$$

such that

$$\sum_{n=1}^{K} a_{i,j,n} = 1, \quad \forall\,(i,j), \quad \text{and} \quad a_{i,j,n} \in \{0,1\}, \quad \forall\,(i,j,n).$$

The norm $\|\,\|$ measures the sum of absolute value of pixel difference between two images. The binary variable encoding here implies that image $I_{i,j,n}$ is selected only when $a_{i,j,n} = 1$. The equality constraint enforces selection of exactly one image at every location. Minimization of the above cost function happens to be a quadratic maximization problem, which, in general, is nondeterministic polynomial-time hard.[21] Thus, even with only pairwise similarity, the image selection problem seems notoriously hard to solve. Our rescue is to approximate the cost and cast it to an optimization for which practical and fast algorithms exist.

We make an approximation of the image selection problem by selecting the images in stages: suppose all the images in $j$'th Z-stack have been selected, we proceed to select images in the $(j+1)$'th Z-stack by minimizing the following cost function:

$$\min \sum_{i} \sum_{n=1}^{K} \sum_{m=1}^{K} a_{i,j+1,n} a_{i+1,j+1,m} (0.5\|I_{i,j} - I_{i,j+1,m}\| + \|I_{i,j+1,m} - I_{i+1,j+1,n}\| + 0.5\|I_{i+1,j} - I_{i+1,j+1,n}\|),$$

where $I_{i,j}$ is the selected image at the $(i,j)$ location. The above cost function has a one-dimensional grid structure, as opposed to 2-D and dynamic programming (DP) can be applied here with a polynomial complexity of $O(MK^2)$ to find out the global minimum.[22] Because we have to run DP for each of $N$ Z-stacks, the total computational complexity is $O(MNK^2)$.

### 2.7 *Image Registration After Frame Selection*

One widely used method for the registration of temporal image sequence is template matching, such as the ImageJ plug-in StackReg.[23] Our recent study shows that when the image sequence contains periods of short subsequences at varying focal planes, template matching results in inferior performances with large registration errors.[19] Periods with drift in the focal plane exist in our experiments, due in part to the large number of frames in the high-temporal resolution 2-D movies. Thus, the template matching methods are unsuitable for this application. To remedy this, we devised a novel image sequence method based on minimum spanning trees (MSTs) algorithm.[19] The underlying graph here consists of $N$ nodes corresponding to the image frames selected at $N$ time points. Two nodes are connected in this graph only if they are $\delta$-distance apart along the time scale. $\delta$ is a design parameter, the value of which has been experimentally determined as in our earlier study.[19] The weight of the edge between two graph nodes $I_i$ and $I_j$ is defined as the registration error: $\|I_i - R(I_i, I_j)\| + \|I_j - R(I_j, I_i)\|$. Here, $R(I_i, I_j)$ represents a registration algorithm (e.g., rigid body registration) that registers image $I_j$ to image $I_i$ and returns the registered image $I_j$. The weighted MSTs algorithm[24] determines an MST that can bypass the image frames with poor image quality and contain registration errors in a long image sequence.[19]

This method was extended to 3-D movies. First, each Z-stack is registered individually by our MST algorithm. Then, Z projections of these Z-stacks are computed to form a temporal 2-D image sequence. The MST algorithm is now applied to this 2-D temporal image sequence to compute the final registration.

Movie quality was quantified using the structural similarity (SSIM) score.[25] A movie was acquired without the trigger, and then a second movie was acquired with the trigger in the same location. The triggered movie was then processed using the image selection and registration algorithms. Two hundred

twenty frames from each image series (untriggered, triggered, triggered with image selection, triggered with image selection and registration) were selected. The SSIM score was calculated in MATLAB (Mathworks) using the m-file written by Wang et al.,[25] for each sequential pair of images in each movie (between frames 1 and 2, 2 and 3, etc.) to determine how different each frame is from the previous one in each stage.

### 2.8 *Cell Motion Analysis*

After image selection and registration, cells were tracked in Imaris (Bitplane). In 2-D movies containing migrating monocytes, small round cells were detected using an absolute intensity threshold, and then the position of each cell's centroid was tracked using Imaris's autoregressive motion algorithm. Broken or inaccurate tracks were corrected manually. Only cells that showed visible net motion during the movie were tracked to ensure the removal of GFP+ macrophages from analysis (the slowest average velocity detected was 10 $\mu$m/ min). Cells were tracked for the length of the entire movie unless they left the field-of-view or the focal plane. Occasionally, additional registration was performed in Imaris to remove sharp changes in the cell tracks. In 3-D movies, round macrophages were tracked automatically using Imaris' surface algorithm, while dendritic-shaped cells were analyzed manually using Imaris' filament tracer algorithm.

## 3 Results

### 3.1 *Plaque Develops Reliably in the External Carotid Artery*

The EC artery, specifically near the branch points of the ST and AP arteries, reliably develops plaque [Fig. 2(a)]. Serial sectioning revealed that plaque is present throughout all branches of this artery (including ST and AP), though with varying compositions in different locations. We analyzed serial sections obtained at 30 $\mu$m intervals from an *Apoe*$^{-/-}$ mouse fed WD 9 weeks. Immunofluorescence revealed CD11b+, CD11c+, and double positive cells as expected [Fig. 2(f)].[26] $\alpha$SMA staining revealed the medial layers and CD31 stained the endothelial monolayer enclosing the lumen [Fig. 2(g)]. To visualize cellular composition by histology, we used H&E staining [Figs. 2(b) and 2(d)]. Neutral lipids were stained with Oil Red O [Figs. 2(b) and 2(c)] and collagen and elastin fibers were stained with trichrome [Figs. 2(b) and 2(e)]. The classical histology staining methods confirmed the presence of atherosclerotic lesions defined as accumulation of lipids, infiltration of immune cells, and thickening of the artery wall.

### 3.2 *Cardiac Triggering and Image Postprocessing Improves Movie Quality*

The cardiac triggered imaging system was first tested using *Apoe*$^{-/-}$ *Cd11c*$^{YFP}$ mice, which have fluorescent myeloid cells

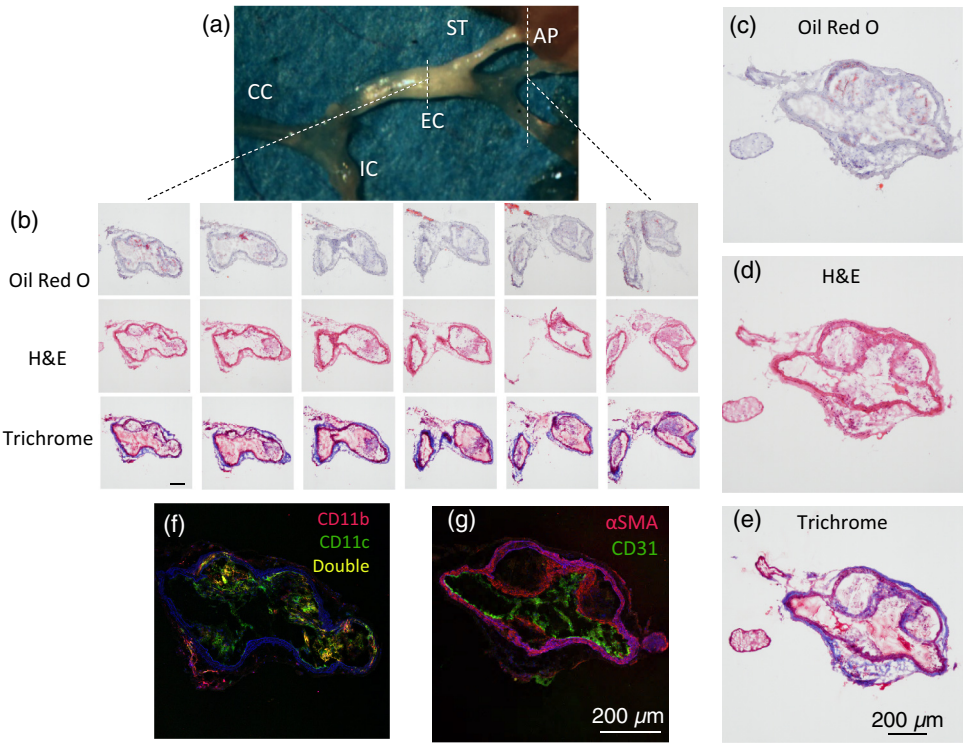


**Fig. 2** (a) Plaque is visible (opaque white) in the external carotid (EC) artery and superior thyroid artery branch of an *Apoe*$^{-/-}$ mouse fed WD for 12 weeks. Plaques can also develop in the ascending pharyngeal artery and lower EC branches. CC, common carotid artery; IC, internal carotid artery. (b) Serial sections every 60 $\mu$m from an *Apoe*$^{-/-}$ mouse fed WD 9 weeks were stained for neutral lipids (Oil Red O), cell components (H&E), and collagen and elastin fibers (Trichrome.) Scale bar = 200 $\mu$m. Every other stained section is shown. Larger examples are shown for visibility (c-e). Serial sections were also immunostained for (f) CD11b and CD11c and (g) $\alpha$-smooth muscle actin and CD31. Autofluorescence and nuclei (stained with Yoyo-1) appear in blue. Brightness was increased by 40% on all fluorescence images for visibility.

in their arterial walls.[26] In addition to the YFP signal, collagen was visualized through SHG.[27] Triggered acquisition greatly reduced motion artifacts compared to untriggered movies [Figs. 3(a) and 4]. However, even with cardiac triggering, residual motion of the artery was still visible. Movie quality was further improved by our automated frame-dropping algorithm. We acquired three frames in three consecutive heartbeats with a pause between sets of images. One "best" image from each set of frames was selected by minimizing a cost function based on the sum of absolute differences of pixel values between the images. Final image stabilization was accomplished by image registration correcting for translation and rotation (Fig. 4). The triggered acquisition, frame selection, and correction for residual translation resulted in image series that were steady. Based on the SSIM score,[25] the triggered acquisition provided the most benefit, followed by the frame selection, with the final correction for translational movement adding further image stabilization [Fig. 3(c)].

### 3.3 *High Frame-Rate 2-D Imaging*

To investigate inflammatory cell recruitment from the lumen, high frame-rate 2-D imaging in a single plane is most suitable.[12] Monocytes are relevant to atherosclerosis and are known to roll in the carotid arteries of *Apoe*$^{-/-}$ mice *in vivo* and *ex vivo*.[28–30] Triggered multiphoton imaging of atherosclerotic live EC arteries of *Apoe*$^{-/-}$ mice resulted in movies with a frame rate of 0.66 Hz that were up to 45-min long. We imaged *Apoe*$^{-/-}$ *Cx3cr1*$^{GFP/+}$ mice that express GFP on various cell types, including blood monocytes and tissue macrophages, as well as small subsets of other immune cells.[16,18] In seven out of eight imaged mice, we found patrolling[31] monocytes on the luminal side of the vessel. Figure 5(a) shows example frames acquired from an *Apoe*$^{-/-}$*Cx3cr1*$^{GFP/+}$ mouse with four patrolling monocytes, three moving with the direction of flow and one moving against the flow [Figs. 5(b) and 6]. Cells flowing in the blood adjacent to the tracked cells are visible, suggesting that the monocytes are on the endothelial surface. This patrolling behavior has previously been described in microvessels[31,32] but not large arteries.

### 3.4 *3-D Multicolor Imaging*

Macrophages are a common cell type in atherosclerotic plaque in *Apoe*$^{-/-}$ mice.[26,33] To demonstrate 3-D imaging of these cells within atherosclerotic plaques, we generated *Apoe*$^{-/-}$*Cx3cr1*$^{GFP/+}$*Cd11c*$^{YFP}$ mice. In the plaque, these mice have fluorescent subsets of macrophages and dendritic cells. Z-stacks were acquired covering one quarter of the circumference of the artery, imaging up to 200 $\mu$m deep [Fig. 7]. In one representative example, stacks were collected in 42-s intervals, producing a four-dimensional representation of fluorescently labeled macrophages moving within the plaque [Fig. 8]. The quality of 3-D movies acquired from live mice [Fig. 9(a)] was comparable to those previously obtained from explanted aortas.[26] The visualized cells are interior to the collagen, but no blood flow is visible in the same focal plane, suggesting that these cells are within the intimal plaque. Some YFP+ fluorescent cells migrated within the plaque [Fig. 9(b)] while other GFP+ or GFP+YFP+ dendritic-shaped cells exhibited "dancing on the spot"-type behavior with extensions and contractions of cell processes and little centroid motion [Fig. 9(c)].

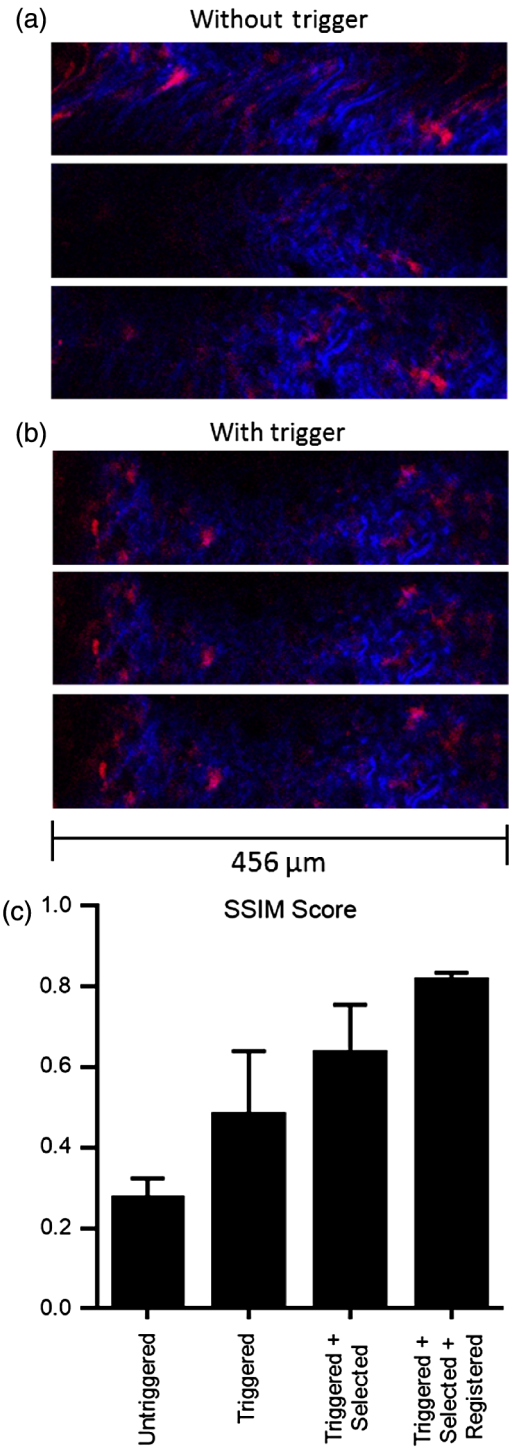


**Fig. 3** (a, b) Example images showing the effect of triggered image acquisition on data quality. (a) Three sequential images freely acquired from an *Apoe*$^{-/-}$ *Cd11c*$^{YFP}$ mouse. (b) Three sequential images acquired using the trigger as described. Red—YFP+ cells and blue—collagen visualized through SHG. See Video 1 for corresponding movies. (c) Pairwise structural similarity scores for image sequences taken from the same location of an *Apoe*$^{-/-}$ *Cd11c*$^{YFP}$ mouse and processed in various ways. The image sets that were analyzed were: free, untriggered acquisition, triggered acquisition, triggered images with the image selection algorithm described in the text, and triggered, selected images with additional registration. Data shows mean (±standard deviation).

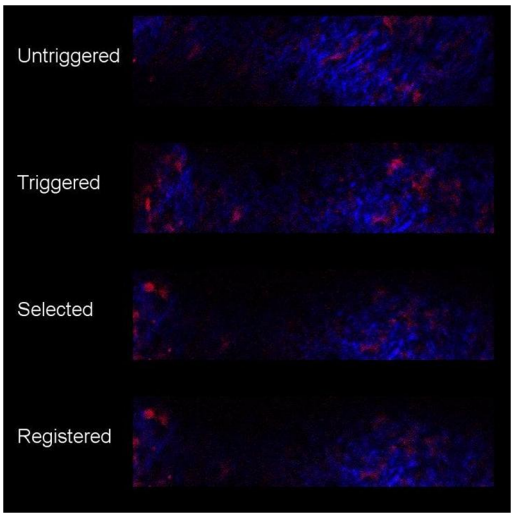


**Fig. 4** Example movies taken from an *Apoe*$^{-/-}$ *Cd11c*$^{YFP}$ mouse. The first (untriggered) was freely acquired without use of the triggering system. Frames were acquired at 24.3 Hz, and are played at real time. The second (triggered) was acquired in the same location, using the triggering system described in Fig. 1. Acquisition rate matched the mouse's heart rate at approximately 3.7 Hz, but is played sped up by 6.7×. The third (selected) is the result of using the image selection algorithm on the triggered movies, and is played at the same frame rate as the triggered movie. The last (registered) is the result of using the minimum spanning tree (MST) registration on the frame-selected movie, and is played at the same frame rate. (Video 1, MPEG, 4.85 MB) [URL: http://dx.doi.org/10.1117/1.JBO.20.2.026005.1].

## 4 Discussion

The ILTIS system developed here successfully images leukocytes in the lumen and atherosclerotic plaques of arteries in live mice. Combining a cardiac trigger and image postprocessing allows for high spatial- and time-resolution imaging of the beating EC artery and its branches without risking tissue damage from mechanical stabilization or altering the artery's native movement. Importantly, we were able to keep the thin fascia overlying this artery in place, thus protecting the vessel wall from surgical trauma. Squeezing the artery has been shown to cause cell death and matrix damage,[11] which can be avoided by triggered acquisition without mechanical stabilization. The resolution with ILTIS allowed not only the tracking of cell movement but also detailed analysis of cell shapes over time. A large volume of tissue can be imaged (up to 200 $\mu$m deep) with minimal registration artifacts. Additionally, this technique is reproducible and can reliably produce stable movies. Simple custom circuitry was built, but no highly specialized equipment is needed.

ILTIS has two modes of operations, 2-D and 3-D, useful for studying different processes. The high time-resolution 2-D imaging is ideal for studying fast cells on the endothelial surface. The number of frames per set and delays between sets can be optimized. Optimal time resolution can be achieved by acquiring one frame per heartbeat, resulting in 4 to 6 frames/s, though this comes at a cost of photobleaching. Alternatively, photobleaching can be minimized by imaging less frequently. Here, we used a net frame rate of 0.66 Hz, which can allow for up to 30 min of useful imaging time without detectable photobleaching. Using *Apoe*$^{-/-}$ *Cx3cr1*$^{GFP/+}$ mice, we used 2-D imaging to demonstrate that monocytes actively crawl both with and against blood flow in large, atherosclerotic arteries.

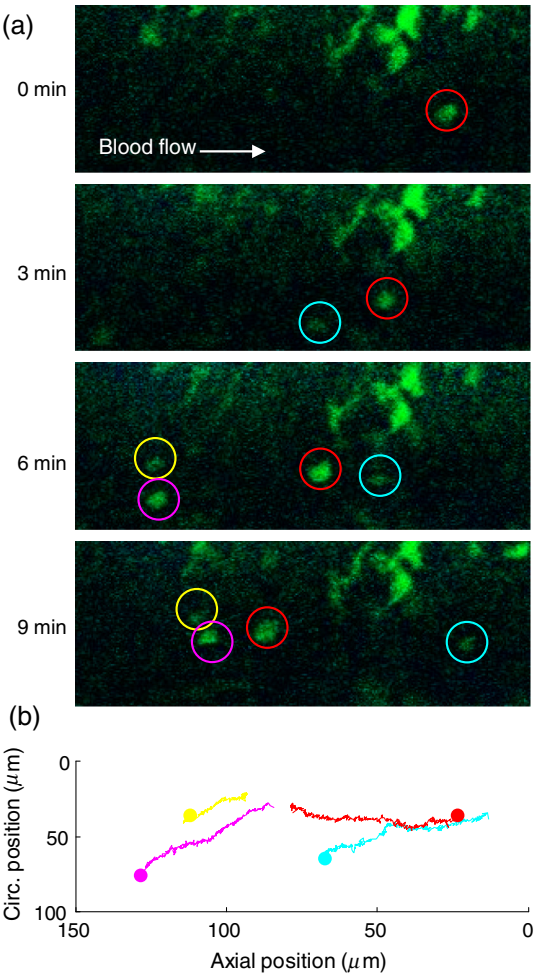


**Fig. 5** (a) Time series of monocytes moving along the lumen of the EC artery of a live *Cx3cr1*$^{+/GFP}$ *Apoe*$^{-/-}$ mouse fed WD for 4 months. Images were acquired at approximately 2 Hz as depicted in Fig. 1 and then selected and registered as described in the text. Four crawling cells were tracked. Blood flow is left to right. Green—GFP+ monocytes and macrophages and blue—collagen in the adventitia visualized through SHG. (b) The positions of the four tracked cells over the 9 min movie. The dot shows the starting position of each cell, color coded by the box they are marked with.

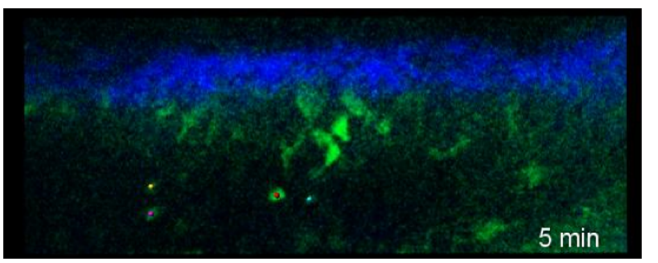


**Fig. 6** Single Z plane movie of the EC artery of a live *Cx3cr1*$^{+/GFP}$ *Apoe*$^{-/-}$ mouse fed WD for 4 months. Images were acquired at approximately 2 Hz (three triggered frames in 600 ms, followed by 1 s pause). Image selection and registration were applied to minimize movement artifacts, reducing the frame rate to 0.66 Hz. Colored dot shows tracked cell centroid. Green—GFP+ cells and blue—collagen visualized by SHG. (Video 2, MPEG, 2.34 MB) [URL: http://dx.doi.org/10.1117/1.JBO.20.2.026005.2].

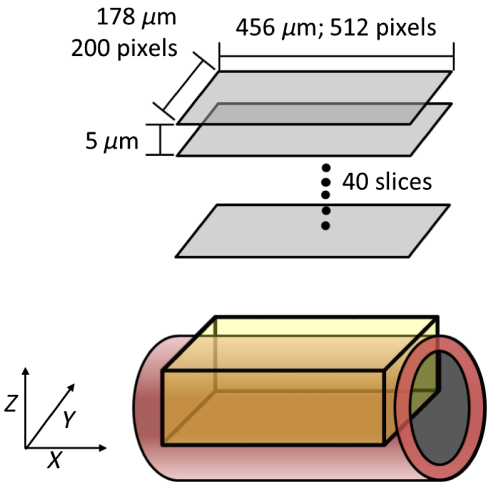


**Fig. 7** Typical size and location of imaged volume (yellow box), which captures 1/4 of the circumference of the arterial wall.

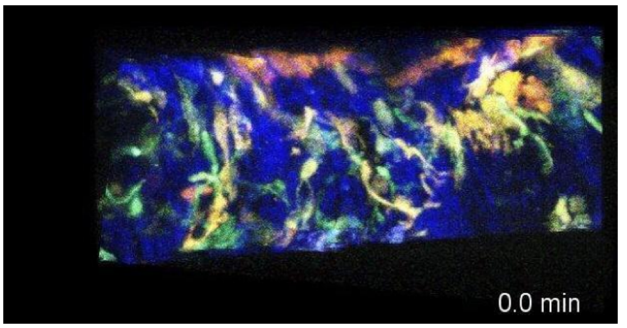


**Fig. 8** Maximum intensity Z projections of the 3-D movie of live *Cx3cr1*$^{+/GFP}$ *Cd11c*$^{YFP}$ *Apoe*$^{-/-}$ mouse fed WD for 5 months. Images were collected using triggered acquisition, and then image selection and registration were applied for stabilization. Stacks were acquired 42 s apart, video played at 15 Hz. Green—GFP+ cells; orange—YFP+ cells; and blue—collagen visualized by SHG. (Video 3, MPEG, 1.41 MB) [URL: http://dx.doi.org/10.1117/1.JBO.20.2.026005.3].

Three-dimensional imaging is suitable for imaging cells within the thick intimal plaque, which move slower but in all three directions. We used ILTIS to show that intravascular YFP+ macrophages were able to migrate within the plaque and GFP+ and GFP+YFP+ cells "danced on the spot," where there was motion of the cell's dendrites but little net centroid motion. This behavior has previously been reported in aortic explants.[26] Our work shows, for the first time, that this type of cell movement occurs in atherosclerotic plaques *in vivo*.

For all imaging, rectangular fields-of-view were chosen to minimize acquisition time of each frame, and the *X*-axis (scan direction) was aligned with the direction of blood flow. There are multiple settings that can be optimized for ideal speed, spatial resolution, and image stability, including the pause after systole is detected before acquiring a frame, the number of line scan averages, the number of lines scanned in the *Y*-direction, the number of replicate frames taken in each Z slice or between pauses, and the length of the pause. Our goal was to maximize the signal-to-noise ratio and the size of the field of view, while ensuring that all frames were entirely taken during effective diastole. We found that our acquisition parameters were best suited for mice with a heart rate of 300 to 350 bpm.

Intravital imaging of large arteries is an invaluable tool for studying leukocyte activity in atherosclerosis. ILTIS will be helpful for answering pertinent open questions in the field, including monocyte recruitment and transmigration, macrophage and dendritic cell activity, and motion of other immune cells.

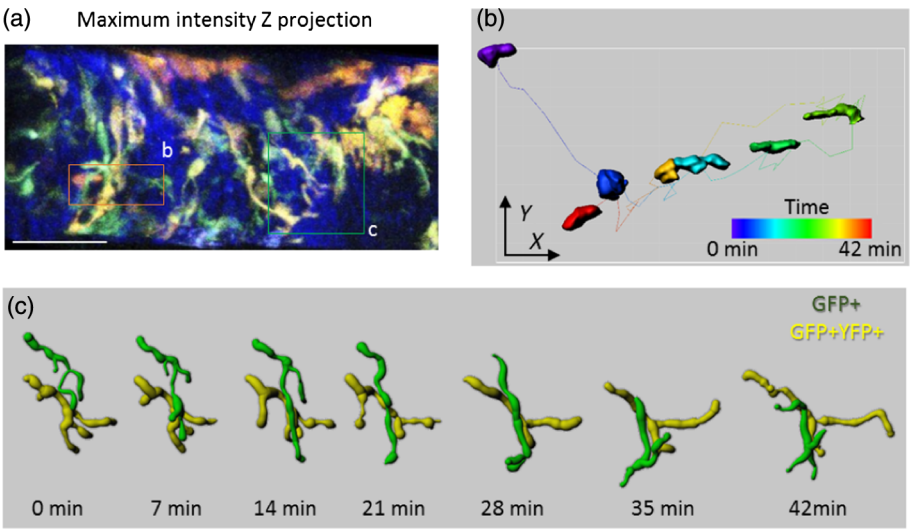


**Fig. 9** (a) Maximum intensity Z projection of a single time point of the 3-D movie of the EC artery of a live *Cx3cr1*$^{+/GFP}$ *Cd11c*$^{YFP}$ *Apoe*$^{-/-}$ mouse fed WD for 5 months with representative moving cells highlighted (boxes). Scale bar = 100 μm. Green—GFP; orange—YFP; and blue—collagen visualized by SHG. See Video 3 for corresponding time lapse recording. (b) Shape and location of an YFP+ cell in orange box in (a) was tracked in Imaris over 42 min, color coded by time. Cell size is decreased to enable visualization of cell shape at all time points. (c) Shape changes of two intertwining dendritic-shaped GFP+ (green) and GFP+YFP+ (yellow) cells in green box in (a) was tracked in Imaris over time.

## Acknowledgments

We thank M. Chadwell (La Jolla Institute) for expert sectioning and histological staining. We thank H. Ouyang and J. Miller (La Jolla Institute) for their outstanding technical help in maintaining the mouse colony. This work was funded by NIH R01 (115232) to K.L. and AHA (#11PRE7580009), HHMI (56005681), and NHLBI (T32HL105373-03) to S.M.

## References

1. H. Ait-Oufella et al., "Adaptive (T and B cells) immunity and control by dendritic cells in atherosclerosis," *Circ. Res.* **114**(10), 1640–1660 (2014).
2. C. Vinegoni et al., "Advanced motion compensation methods for intravital optical microscopy," *IEEE J. Sel. Topics Quantum Electron.* **20**(2), 1–9 (2014).
3. S. Lee et al., "Real-time in vivo imaging of the beating mouse heart at microscopic resolution," *Nat. Commun.* **3**, 1054 (2012).
4. C. Vinegoni et al., "Sequential average segmented microscopy for high signal-to-noise ratio motion-artifact-free in vivo heart imaging," *Biomed. Opt. Express* **4**(10), 2095–2106 (2013).
5. W. Li et al., "Intravital 2-photon imaging of leukocyte trafficking in beating heart," *J. Clin. Invest.* **122**(7), 2499–2508 (2012).
6. S. Lee et al., "Improved intravital microscopy via synchronization of respiration and holder stabilization," *J. Biomed. Opt.* **17**(9), 096018 (2012).
7. R. Chevre et al., "High-resolution imaging of intravascular atherogenic inflammation in live mice," *Circ. Res.* **114**(5), 770–779 (2014).
8. K. Jung et al., "Endoscopic time-lapse imaging of immune cells in infracted mouse hearts," *Circ. Res.* **112**(6), 891–899 (2013).
9. M. R. Looney et al., "Stabilized imaging of immune surveillance in the mouse lung," *Nat. Methods* **8**(1), 91–96 (2011).
10. C. Vinegoni et al., "Motion compensation using a suctioning stabilizer for intravital microscopy," *Intravital* **1**(2), 115–121 (2012).
11. R. T. Megens et al., "In vivo high-resolution structural imaging of large arteries in small rodents using two-photon laser scanning microscopy," *J. Biomed. Opt.* **15**(1), 011108 (2010).
12. M. Drechsler et al., "Hyperlipidemia-triggered neutrophilia promotes early atherosclerosis," *Circulation* **122**(18), 1837–1845 (2010).
13. D. Soulet et al., "Automated filtering of intrinsic movement artifacts during two-photon intravital microscopy," *PLoS One* **8**(1), e53942 (2013).
14. M. Phillipson et al., "Intraluminal crawling of neutrophils to emigration sites: a molecularly distinct process from adhesion in the recruitment cascade," *J. Exp. Med.* **203**(12), 2569–2575 (2006).
15. Y. Nakashima et al., "ApoE-deficient mice develop lesions of all phases of atherosclerosis throughout the arterial tree," *Arterioscler. Thromb.* **14**(1), 133–140 (1994).
16. S. Jung et al., "Analysis of fractalkine receptor CX(3)CR1 function by targeted deletion and green fluorescent protein reporter gene insertion," *Mol. Cell. Biol.* **20**(11), 4106–4114 (2000).
17. R. L. Lindquist et al., "Visualizing dendritic cell networks in vivo," *Nat. Immunol.* **5**(12), 1243–1250 (2004).
18. L. Landsman et al., "Cx3cr1 is required for monocyte homeostasis and atherogenesis by promoting cell survival," *Blood* **113**(4), 963–972 (2009).
19. S. McArdle et al., "Registering sequences of in vivo microscopy images for cell tracking using dynamic programming and minimum spanning trees," in *IEEE Int. Conf. on Image Processing*, IEEE, Paris, France (2014).
20. S. Z. Li, *Markov Random Field Modeling in Image Analysis*, Springer, London, England (2009).
21. R. Horst and H. Tuy, *Global Optimization Deterministic Approaches*, Springer, Heidelberg, New York (1996).
22. D. P. Bertsekas, *Dynamic Programming and Optimal Control*, 2nd ed., Athena Scientific, Belmont, Massachusetts (2000).
23. P. Thevenaz, U. E. Ruttimann, and M. Unser, "A pyramid approach to subpixel registration based on intensity," *IEEE Trans. Image Process.* **7**(1), 27–41 (1998).
24. T. H. Cormen et al., *Introduction to Algorithms*, 2nd ed., MIT Press and McGraw-Hill, Cambridge, Massachusetts (2001).
25. Z. Wang et al., "Image quality assessment: from error visibility to structural similarity," *IEEE Trans. Image Process.* **13**(4), 600–612 (2004).
26. E. K. Koltsova et al., "Dynamic T cell-APC interactions sustain chronic inflammation in atherosclerosis," *J. Clin. Invest.* **122**(9), 3114–3126 (2012).
27. W. R. Zipfel et al., "Live tissue intrinsic emission microscopy using multiphoton-excited native fluorescence and second harmonic generation," *Proc. Natl. Acad. Sci. U. S. A.* **100**(12), 7075–7080 (2003).
28. Y. Huo et al., "The chemokine KC, but not monocyte chemoattractant protein-1, triggers monocyte arrest on early atherosclerotic endothelium," *J. Clin. Invest.* **108**(9), 1307–1314 (2001).
29. Y. Huo, A. Hafezi-Moghadam, and K. Ley, "Role of vascular cell adhesion molecule-1 and fibronectin connecting segment-1 in monocyte rolling and adhesion on early atherosclerotic lesions," *Circ. Res.* **87**(2), 153–159 (2000).
30. Y. Huo et al., "Circulating activated platelets exacerbate atherosclerosis in mice deficient in apolipoprotein E," *Nat. Med.* **9**(1), 61–67 (2003).
31. C. Auffray et al., "Monitoring of blood vessels and tissues by a population of monocytes with patrolling behavior," *Science* **317**(5838), 666–670 (2007).
32. L. M. Carlin et al., "Nr4a1-dependent Ly6C(low) monocytes monitor endothelial cells and orchestrate their disposal," *Cell* **153**(2), 362–375 (2013).
33. E. Galkina et al., "Lymphocyte recruitment into the aortic wall before and during development of atherosclerosis is partially L-selectin dependent," *J. Exp. Med.* **203**(5), 1273–1282 (2006).

**Sara McArdle** received a BS degree in biomedical engineering from Columbia University in 2009. She is currently a PhD candidate at the University of California, San Diego, in the Department of Bioengineering, with a specialization in multiscale biology. She is completing her PhD research at the La Jolla Institute for Allergy and Immunology in the Division of Inflammation Biology with Dr. Klaus Ley.

**Grzegorz Chodaczek** is a head of the Confocal Microscopy Laboratory at the Wroclaw Research Centre EIT+, Wroclaw, Poland. He received his PhD degree in immunology from the Institute of Immunology and Experimental Therapy in Poland. Between 2007 and 2011, he was a postdoctoral fellow at MD Anderson Cancer Center at Houston, Texas, USA, and until March 2014, he was a microscopy core manager at the La Jolla Institute. His research focuses on intravital imaging of immunological processes.

**Nilanjan Ray** received his B.M. Engg. from Jadavpur University, India, in 1995, his MTech degree from CS Indian Statistical Institute, Calcutta, India, in 1997, and his PhD degree in E. Engg. from the University of Virginia in 2003. He is an associate professor in the Department of Computing Science, University of Alberta, Canada. His research area is image and video analysis: image segmentation, registration, tracking, and motion analysis. He has coauthored two monographs—*Biomedical Image Analysis: Tracking* and *Biomedical Image Analysis: Segmentation*, Morgan & Claypool Publishers.

**Klaus Ley** received his MD degree in 1982 followed by postdoctoral training in Berlin and San Diego. In 1994, he became professor of biomedical engineering and later director of the Robert M. Berne Cardiovascular Research Center at the University of Virginia. In 2007, he became a professor and founding head of the Division of Inflammation Biology at the La Jolla Institute. He received the 2008 Bonazinga and the 2010 Malpighi awards.